Composite Structures 331 (2024) 117887

Contents lists available at ScienceDirect

Composite Structures

journal homepage: www.elsevier.com/locate/compstruct

Experimental and numerical analysis of the Microstructure and mechanical properties of unidirectional glass fiber reinforced epoxy composites

Seshaiah Turaka [a], Ravikiran Chintalapudi [b], Narayanan Kannaiyan Geetha [c], Bridjesh Pappula [b], Seshibe Makgato [d,*]

[a] Department of Mechanical Engineering, QIS College of Engineering and Technology, Ongole 523272, India
[b] Department of Mechanical Engineering, MLR Institute of Technology, Hyderabad 500043, India
[c] Department of Mathematics, Dayananda Sagar College of Engineering, Bengaluru 560078, India
[d] Department of Chemical Engineering, College of Science, Engineering and Technology, University of South Africa (UNISA), C/o Christiaan de Wet & Pioneer Avenue, Florida Campus, 1710 Johannesburg, South Africa

ARTICLE INFO

Keywords:
GFRP composites
Fiber orientation
Mechanical properties
Microstructure
Finite element analysis
Von Misses stresses

ABSTRACT

This paper proposes a numerical model to predict the pattern and features of the fracture surface and to understand the mechanisms and cause of the failure. Various fiber orientations of 0°, 90°, 0°/90° and ± 45° were utilized in the production of unidirectional glass-fiber-reinforced epoxy composites via the vacuum bagging technique. The mechanical properties of the manufactured composites were evaluated by measuring parameters including tensile strength, compressive strength, flexural strength and interlaminar shear strength. High-resolution scanning electron microscopy was used to examine the mechanisms of fracture in laminates. The mechanical properties of the composite material were found to be considerably improved when a unidirectional 0° fiber orientation was used, as compared to other fiber orientations. This was true for tensile, compressive, flexural and interlaminar shear loading modes. The composite laminates demonstrated several modes of breaking, including fibers pulling away from the matrix, holes in the matrix and river flow lines, depending on the direction of the fibers. The outcomes of the numerical simulation demonstrate a high level of fidelity with experimental findings. This study provides a valuable reference for predicting numerical analysis of the microstructure and mechanical properties.

1. Introduction

Composites with a fiber-reinforced polymer matrix have high strength, low weight and increased rigidity. Fiber-reinforced composites fail because of fiber fractures, delamination and matrix fractures. Moreover, laminated composites are delaminated, losing rigidity and failing as a result of a lack of inter-laminar strength. Fiber-reinforced thermoset polymer matrix composites are generally used in automotive, aerospace, marine, sports and medical applications [1,2]. In view of the fact that there is a strong interlocking between glass fiber (GF) and resin, treating GF's surface with colloidal silica or silane particles can enhance the composite's properties. Safi et al. [3] studied the impact of interface modification on the adhesion and tensile properties of GF/epoxy composites using colloidal nanosilica particles and a new silane-coupling agent blend. This improved the tensile strength and ductility of the fibres. In their study, Loganathan et al. [4] subjected Unidirectional Glass Fiber Reinforced Epoxy Composites (UD-GFRECs) to continuous cycle loadings. Compared to other stacking sequences, 0°/90°/0°/90° laminates are effective at dissipating energy. The study conducted by Li et al. [5] on UD-GFREC laminates (0°, 90°, 45° or −45°) revealed that a 45° fiber orientation significantly improved shear properties across various temperatures under compressive loads.

Researchers have also tried to use finite element analysis (FEA) to predict the tensile properties of GFs that are oriented in a single direction and then compared their predictions with actual tensile strength results. For example, Dahshan et al. [6] compared woven roving glass fiber reinforced epoxy composites (GFREC) and cross-ply laminates. They discovered that GFREC has superior tensile strength and inter-laminar fracture resilience. Fathollah et al. [7] optimized compressive and in-plane shear strength in Glass Fiber-reinforced Polymer (GFRP) composites by utilizing various fiber volume fractions. They found that the amount of composite fibers and in-plane loading influence compressive and in-plane shear behavior. Cao [8] showed a 3D printing

* Corresponding author.
E-mail address: makgato2001@yahoo.com (S. Makgato).

https://doi.org/10.1016/j.compstruct.2024.117887
Received 23 August 2023; Received in revised form 27 November 2023; Accepted 5 January 2024
Available online 6 January 2024

Nomenclature

Parameter	Description
CFREC	Carbon fiber-reinforced composite
FE	Finite element
FEA	Finite element analysis
GF	Glass fiber
GFREC	Glass fiber-reinforced epoxy composites
GFRP	Glass fiber-reinforced polymer
ILSS	Inter laminar shear strength
SEM	Scanning electron microscope
UD-GFREC	Unidirectional glass fiber reinforced epoxy composites
UTS	Ultimate tensile strength (MPa)
σ_F	Flexural stress (MPa)
W	Applied load (N)
L	Length of the specimen (mm)
b	Width of the specimen (mm)
t	Thickness of the specimen (mm)
d	Gauge length of the specimen (mm)
E_F	Flexural Modulus (GPa)
m	Slope of load deflection curve (N/mm)
ε_F	Flexural strain
d_{max}	Max. beam deflection (mm)
τ_w	Shear load
τ_s	Shear strength
G_s	Shear modulus
γ_{xy}	Shear strain displacement

method that used three types of filament: carbon nanotube/polylactic acid, continuous carbon fiber (CF) and polylactic acid (PLA). These filaments increased buckling loads and changed how continuous CF behaved under buckling loads. While buckling load with polylactic acid CF/PLA was significantly enhanced with 20 % (by weight) carbon nanotubes. In a separate case, Cao et al [9] used PLA as the core material and sandwiched in between glass fiber-reinforced polymer (GFRP) skins and found a correlation between in-plane shear, out-of-plane shear strain and specific peak bending load. The results showed that 3D-printed PLA core for composite sandwich structures was enhanced by ~34 % (in-plane shear strength)/~29 % (modulus), ~25 % (out-of-plane shear strain/~31 % (modulus) and ~19 % (specific peak bending load) than balsa core sandwich composites at optimized resin by 20.43–22.86 wt%. In another case, Cao [10] used fusion joining to improve low-temperature issues in a carbon fabric heating element by interlacing two layers of multi-walled carbon nanotube sheets. Six different heating element sizes were studied, and the experimental results showed that the strength has increased by 49.9 %, 71.5 %, 84.1 %, 110.5 %, 118.2 % and 153.6 %, respectively [10]. Mary et al. [11] identified the damage behavior of cross-ply laminates using optical microscopy and ultrasonic scanning. Ultrasonic scans disclosed delamination and fissures in fiber composites. Sharma et al. [12] investigated the computational and experimental mechanical parameters of GFRECs subjected to different mechanical loads. Ahmed et al. [13] observed the enhancement in GFRECs using nanoclays with a filler content of 2 wt%: 11 % on Ultimate Tensile Strength (UTS), 15 % on tensile modulus and 43 % fracture toughness. According to Khademi et al. [14], fiber treated with graphene oxide increased the interlaminar shear strength of GFREC. Mohammad et al. [15] investigated the warp/fill strength and rigidity of GFRECs in three fabric constructions with harnesses (2, 5 and 8). The integration of two GFREC composites improved their tensile and elastic modulus. Khademi et al. [14] investigated how micromechanical models can be used to estimate the strength and rigidity of unidirectional GFRECs subjected to dynamic strain rate loading. Shanti Kiran et al. [16] investigated the effect of nanoclay on the tensile and flexural behavior of GFREC in which, UTS has significantly enhanced at 31.5 % volume of glass fiber with 0 % (by weight) nanoclay.

Different researchers investigated carbon fiber-reinforced polymer composite laminates, hybrid fiber-reinforced composites and powder epoxy resin-based unidirectional composite materials [17–25]. For example, Kim et al. [17] fabricated hybrid-fiber-reinforced composites using vinyl ester resin with flax, carbon and glass fibers. They incorporated flax fibers to reduce cost, weight, enhance the mechanical properties and environmental effects. The experimental results showed that flax/glass/carbon/vinyl ester resin composites had the highest flexural strength of 729 MPa and impact strength of 0.17 J/mm^2 than the flax/glass/vinyl ester resin hybrid fiber composites. Chitturi et al. [18] investigated hybrid (glass fiber/polycarbonate) composites with various stacking arrangements. The outcomes of the experiments demonstrated that polycarbonate composites had enhanced impact properties (resistance/energy absorption). Chen et al. [21] fabricated three different fabric structures (75D, 72F and 100D/96F) with polyester-based composites. The results of the experiment revealed that 75D fabric structures have better mechanical properties as compared to other fabric structures (72F and 100D/96F). Behera et al. [22] fabricated and examined carbon fiber-reinforced polymer composite laminates oriented at ± 45° and subjected the laminates to static tension and compression loadings. The experimental results showed that matrix fracture density, residual stiffness, lower energy dissipation obtained in static tension and the lowest probability of matrix crack growth exhibited greater energy parameters as well as lower stiffness degradation obtained in compression. Mamalis et al. [23] fabricated carbon fibers with three sizing agents, such as T700S-24 K-50C, T700S-24 K-F0E and T700S-24 K-60E using 0.3, 0.7 and 1 % sizing agents to create powder epoxy resin-based unidirectional composites. Strength and modulus of CFRECs with a 0.7 % sizing agent have increased by 22 % and 12 %, respectively.

A thorough review of the literature revealed that many studies have been done on the mechanical properties of E-glass fiber composites, mainly focusing on the different fiber orientations [17–25]. Nevertheless, there are no studies that compared experimental and numerical simulations of the tensile, flexural, compressive and inter laminar shear strength (ILSS) behavior of UD-GFRECs with different fiber orientations. Therefore, this study aimed to use numerical modelling to predict features of the fracture surface patterns and failure mechanisms using different fiber orientations. For this reason, the composite laminates are characterized to assess the effect of different glass fiber lamination orientations, such as 0°, 90°, 0°/90° and ± 45° on the mechanical properties (tensile, compressive, flexural and inter-laminar shear strengths) of composite laminates. The study used high-resolution scanning electron microscopy to examine the mechanisms of fracture in laminates.

2. Materials and methods

2.1. Materials and properties

E-glass is reinforced with alumina-borosilicate glass fiber sheets (Arun Textiles, Bangalore, India) and an epoxy polymer resin (Araldite®LY 556, Tirven Industries, Balanagar, Hyderabad, India) matrix. Fibers with circular cross-sections of 0.55–0.77 mm and 235 mm, E-glass fibers of 200 GSM with unidirectional, bi-directional and ± 45° mat types were utilized. The physical and mechanical properties of the matrix material and glass fibers are detailed in Table 1.

2.2. Fabrication of laminated composites

The vacuum bagging technique was utilized to manufacture

Table 1
Physical and mechanical properties of the constituents [26].

Property	E-glass fibers	Epoxy matrix
Volume fraction (V_f, V_m)	0.4	0.6
Density (ρ_f, ρ_m), kg/m^3	2550	1800
Youngs modulus (E_f, E_m), MPa	72,000	4000
Ultimate tensile strength, MPa	1950	100
Tensile modulus, GPa	17.20	7.94
Ultimate tensile strain (%)	2.7	4.4
Compressive strength, MPa	207	110
Compressive modulus, GPa	6.92	5.45
Shear strength, MPa	34	35
Shear modulus, GPa	30	36
Poisson's coefficients	0.22	0.33

composite laminates, as depicted in Fig. 1. In a glass basin, epoxy resin and hardener (Aradur 5052, Tirven Industries, Balanagar, Hyderabad, India) were mixed at a volume ratio of 10:1. Glass fibers of the desired diameters were manually stacked into the mold. To prevent laminate from adhering to the exposed mold surface, a cleansing agent was used. Layers of glass fiber had the same ratio of resin to hardener. The open mold was vacuum compressed at 0.8 bar to bond matrix and fiber and remove air. The laminated composite underwent a 4-hour post-curing at 80 °C after being cured at room temperature.

Four laminated composite specimens of size 300 mm × 300 mm × 3 mm were made by altering fiber orientation at 0° (unidirectional), 90° (transverse), 0°/90° (bidirectional woven fabric) and ± 45° (Fig. 2). Each specimen has 15-layered laminates with 0.2 mm layers and 50 % fiber. Composite specimens with different fiber orientations were characterized by tensile, compressive, flexural and interlaminar shear.

The servo-hydraulic testing apparatus (Model 8801, Instron, Illinois, USA) was used to perform tensile, compressive and flexural characterization and, subsequently, to analyze the stress–strain behavior of laminated composites with varying fiber orientations. The ILSS was determined using a short beam bending test instrument (Model 100 series, ZWICK Roell & Co., GmbH, Germany). The tensile test sample preparation and testing were conducted adapting ASTM D 3039 [27] standard. The tensile test configuration is depicted in Fig. 3(a) with a 2 mm/min load being applied. Fig. 3(b) depicts an extensometer measuring strain. At ambient temperature (relative humidity of 50 %), the average UTS and tensile modulus of five fiber-oriented laminated composites were tested. The compression behavior of test samples was examined adapting ASTM D3410 [28] compression testing standards.

Composites' flexural characteristics are useful for structural applications. The ASTM D790 [29] standard was used to prepare test samples and were subjected to a 3-point flexural bend test at a cross-head speed of 1 mm/min and a span-to-thickness ratio of 16. All test samples were recorded for flexural load and displacement. The test specimen's failure (σ_F) was calculated from its flexural stress modulus (E_F) and strain (ε_F) [30] using Eqs.1 – 3.

$$\sigma_F = \left(\frac{3WL}{2bt^2}\right)\left[1 + 6\left(\frac{d}{L}\right)^2 - 4\left(\frac{d}{L}\right)\left(\frac{t}{L}\right)\right] \quad (1)$$

$$E_F = \frac{mL^3}{4bt^3} \quad (2)$$

$$\varepsilon_F = \frac{6d_{max}}{L^2} \quad (3)$$

Finally, the fractured surface after the mechanical test was analyzed using HR-SEM (Quanta FEG 200). The gold coating with a thickness of ~ 10 nm was provided in the cross-section of each fractured sample at 10 mA for 60 s using a plasma sputter coater (SC7620-CF, Quorum Laughton Lewes).

3. Results and discussions

3.1. Effect of ply orientations on composite specimens

The tensile stress–strain characteristics and uncertainty error of the UD-GFRECs with four different stacking sequences of fiber orientations are presented in Fig. 4(a) and 4(b). It is seen from Fig. 4(a) that the laminated composites in all cases exhibit brittle behavior. There is substantial variation in the tensile strength of composites at different fiber orientations. The tensile strength is found to be highest for unidirectional (0° ply orientation) fiber-oriented composites. This maximum load is carried by the reinforcing fibers and accordingly, the material exhibits high tensile strength but minimal ductility.

The unidirectional orientation of composite fibers causes a sudden failure without plastic deformation. Due to fiber fracture and loss of strength, the matrix could not sustain the strain on its own. A tensile force applied to a composite with transverse fiber orientation (90° ply orientation) causes fiber bending, fracture propagation and crack initiation. Thus, fiber–matrix interface debonding accelerates, reducing the tensile strength of the composite. In the bidirectional cross-woven (0°/90°) direction, fibers bear the greatest load in the longitudinal direction but almost none in the transverse direction. Bidirectional ply orientation reduces the UTS of the laminate, which is found to be lower than at unidirectional ply orientation. At moderate loads, off-axis composite laminates distribute tensile force in an unequal manner and shear in the first interphase matrix. Pierron et al. [31] reported a similar effect for composite laminates with ± 45° fiber orientation. Fig. 4(a) demonstrates that the composite exhibits a dominant and diminished tensile behavior. Table 2 demonstrates the tensile stress–strain results of UD-GFRECs with various fiber orientations. Table 2 indicates that composites with a 0° fiber orientation had the highest average tensile strength and yield strength with a 0.2 % offset, whereas composites with a ± 45° fiber orientation had the lowest. ± 45°, 90° and 0°/90° fiber-oriented specimens have UTS values of 11.93 %, 25.93 % and 62.14 percent,

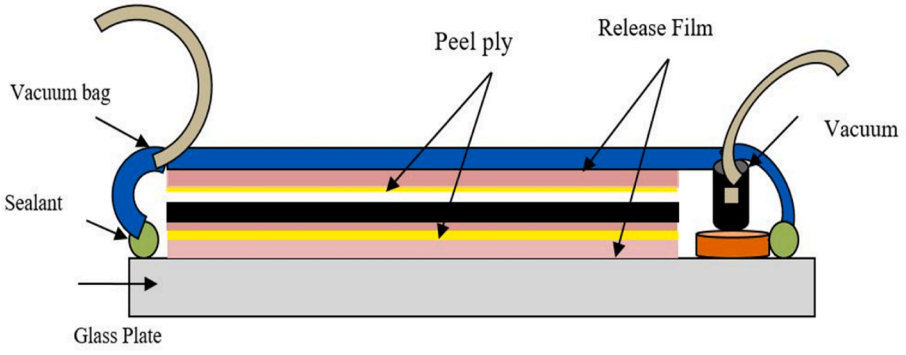

Fig. 1. Schematic diagram of vacuum bagging lay-up technique.

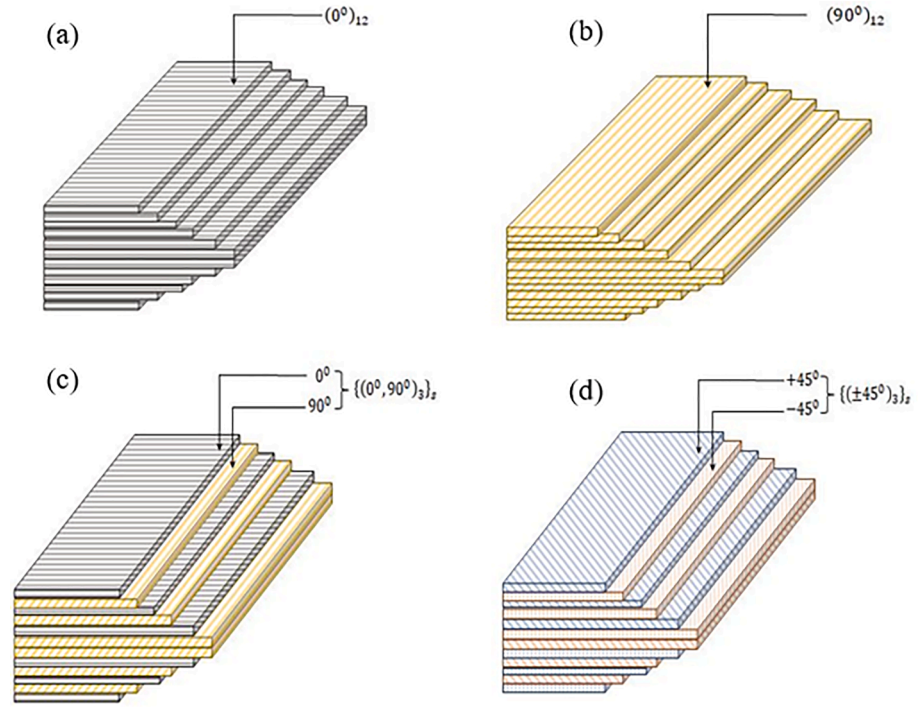

Fig. 2. Laminated composite specimens fabricated at different orientations a) $(0^0)_{12}$, b) $(90^0)_{12}$, c) $\left\{(0^0,90^0)_3\right\}_s$, and d)$\{(\pm 45^\circ)_3\}_s$

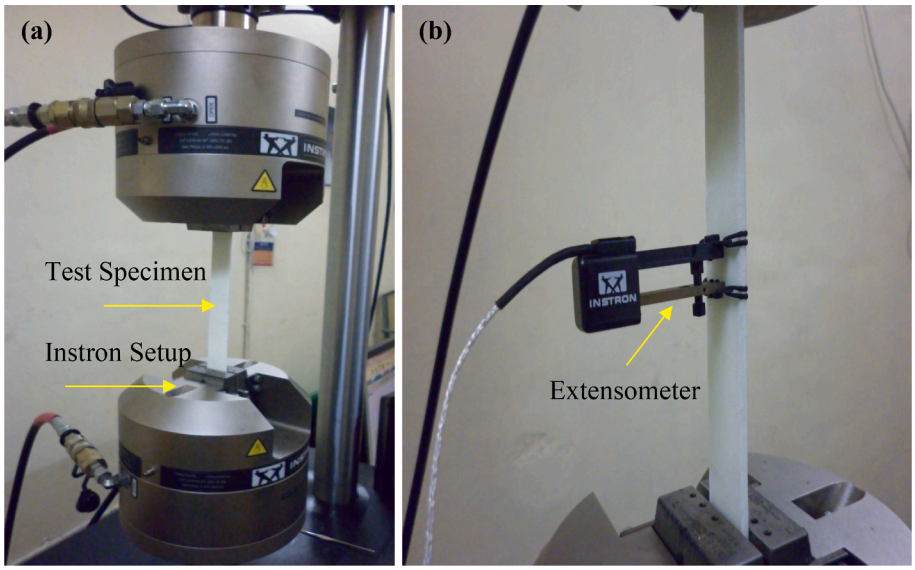

Fig. 3. (a) Experimental arrangement for tensile test, and (b) Extensometer attachment for strain measurement.

respectively, of the 0° specimen. The uncertainty error for UTS of 90°, 0°/90° and ± 45° fiber-oriented specimens is found to be 25.93 %, 11.93 % and 62.14 % of that of the 0° fiber specimens, respectively, as shown in Fig. 4(b). The UTS is greatest for 0° fiber-oriented specimens because the tensile load is transmitted along the fiber axis and is equally distributed. In other fiber orientations, the fiber axis is not parallel to the line of loading action, resulting in fiber pulling-off and premature failure. 0° fiber orientation has the highest yield strength because it resists elastic deformation (Fig. 4(a)).

The compressive stress–strain characteristic and uncertainty error of the developed UD-GFRECs with four different fiber orientations are shown in Fig. 5(a) and 5(b). Fig. 5(a) shows that laminated glass/epoxy composites have nonlinear stress–strain behavior at different ply orientations, and fibers break at all orientations. Researchers discovered that fiber-reinforced composite laminates exhibit nonlinear behavior [32,33]. In comparison to other fiber orientations, 0° ply-oriented laminated composites have the highest compressive strength of 14.864 MPa while ±45° specimens have the lowest compressive strength of 4.608 MPa. The uncertainty error for compressive strength of 90°, 0°/90° and ± 45° fiber-oriented specimens is found to be 26.17 %, 8.27 % and 68.92 % of that of the 0° fiber specimens, respectively, as presented in Fig. 5(b). In unidirectional laminated composites, robust interface bonding between the matrix and fibers may be the reason why the matrix prevents fiber buckling. Other fiber-oriented composites typically exhibit inadequate fiber–matrix adhesion during curing. Specimens with fiber orientations of 0°/90°, 90° and ± 45° had reduced

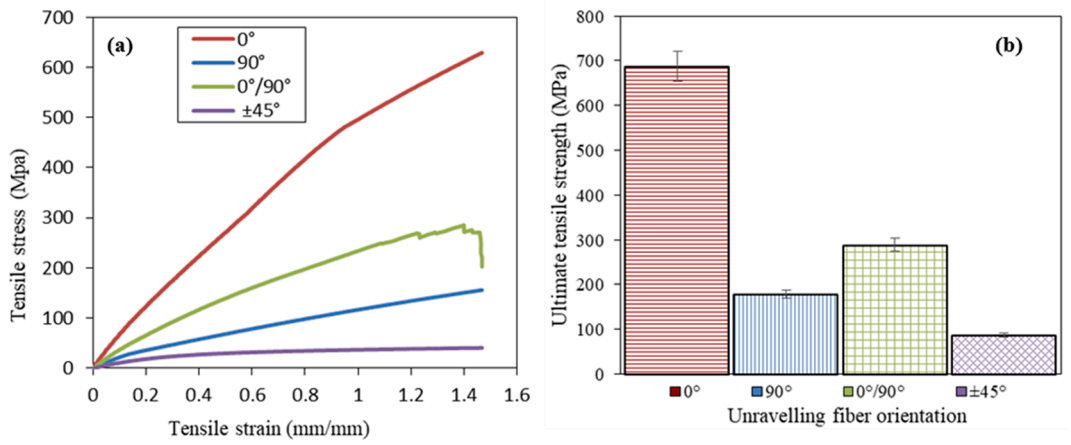

Fig. 4. Characteristic curves of ud-gfrecs (a) tensile stress–strain, (b) Uncertainty error bar.

compressive moduli because of fiber misalignment and shear. This is the moment at which the epoxy matrix starts to crush due to the continued compressive load, resulting in the formation of microcracks inside the matrix.. During this stage, the stress of the composite remains relatively constant, forming a plateau region. This is because the fibers are still intact and bear most of the load, but the epoxy matrix is progressively failing. The plateau represents the composite's ability to maintain load-bearing capacity even as the matrix begins to fail. Eventually, the microcracks in the epoxy matrix accumulate and coalesce, weakening the structure significantly. At this point, the stress starts to decrease as the composite undergoes a catastrophic failure. The fibers can no longer bear the load effectively without the support of the matrix, and the material experiences a rapid drop in stress.

The variation in the flexural strength and uncertainty error of the composite specimens with different fiber orientations is shown in Fig. 6 (a) and 6(b). The flexural strength of the specimen is found to be greater for 0° fiber orientation (129.622 MPa) compared to the other fiber-oriented composite specimens (Table 2). This is due to the maximum load carried by the outermost fibers in unidirectional laminated composites but also in other ply-oriented specimens, as is evident from Fig. 6 (a) and Table 2. The uncertainty error for flexural strength of 90°, 0°/90° and ± 45° fiber-oriented specimens is found to be 90.22 %, 39.77 % and 59.74 % of that of the 0° fiber specimens, respectively, as presented in Fig. 6(b). The load-carrying capacity is reduced because of the inadequate richness of the matrix in the neighboring fibers. Further, the flexural strength of the specimen is found to be at its maximum owing to the appropriate interlocking between the fibers at 0° orientation. However, in the case of 90° orientations, due to the large stress induced by fiber bridging at crack surfaces, the flexural strength is observed to be at its minimum.

Fig. 7(a) and 7(b) show the shear load–displacement characteristic and uncertainty error of the composite specimens with four different fiber orientations, respectively. The profiles of the plots in all the cases show a similar trend. However, the 0° fiber-oriented specimen is noticed to withstand more load, and less load is carried out by the ± 45° oriented specimens with the appearance of sudden failure. The 0°/90° composite is a laminate structure composed of alternating layers of 0° and 90° fiber orientations. This arrangement combines the benefits of both orientations: the 0° layers provide strength and stiffness in one direction, while the 90° layers provide reinforcement in the perpendicular direction. This results in a composite that can effectively resist flexural deformation in two orthogonal planes. Therefore, it exhibits a different behavior in the flexural displacement curve compared to the other oriented specimens. This observation is in good agreement with the findings of Agrawal et al. [34].

Table 2 reveals the shear strength of the composite laminates at different ply orientations, as determined from Fig 7(a). The shear strength of the 0° fiber-oriented laminated composite is observed to be maximum (15.62 ± 3.11 MPa) as compared to the composites prepared at other fiber orientations (minimum for ± 45° fiber-oriented specimens: 10.15 ± 1.21 MPa). The uncertainty error for ILSS strength of 90°, 0°/90° and ± 45° fiber-oriented specimens is found to be 60.53 %, 4.62 % and 47.50 % of that of the 0° fiber specimens, respectively, as shown in Fig. 7(b). There is a small deviation in the values of the shear strength for each specimen, and this is due to the orthotropic nature of the laminate samples. These results correspond with the results obtained by Selmy et al. [35], who disclosed that the UD-GFRECs exhibit higher short beam shear strength as compared to the randomly oriented glass fibers.

3.2. *Fractography of unidirectional –glass epoxy specimens*

Fig. 8 depicts SEM images of fractured composite specimens subjected to varying ply orientations after tensile loading. The fibers in 0° ply-oriented composite specimens are smooth and devoid of matrix adhesion due to delamination, as shown in Fig. 8(a). Interlaminar shear strains result in insufficient tension transfer at the interface [36]. Consequently, the fiber faces undergo localized shearing and matrix/fiber fracture. Fig. 8(b) depicts fiber fracture in the composite with 90° ply pattern. Due to insufficient interlocking or interlayer porosity, fibers detach from the matrix and deform [37]. Fig. 8(c) displays fiber bunch pullout voids, verifying debonding at the fiber–matrix interface. The tensile strain is absorbed by fibers parallel to the load axis in the 0°/90° ply composite specimen. During tensile loading, weaker fiber–matrix interfacial bond strength causes fiber bundle detachment as shown in Fig. 8(d) which reduces the strength but increases the ductility. By drawing out fiber bundles, the free lateral edges influence the deeply buried pockets generated at the sample's lateral edge.

Fig. 9 shows that SEM images of compressively loaded specimens with varying fiber orientations reveal distinct fracture patterns. Fig. 9(a) depicts fibers with no fractures whereas, in composite specimens with 0° ply orientation, the fiber pulls out and the matrix fracture is virtually nonexistent, indicating strong matrix-fiber interfacial adhesion. The debonding of flat surface fibers is depicted in Fig. 9(b). The morphology of Fig. 9(a) is distinguished by crack bridging and fiber–matrix fracture resulting from feeble interfacial connections. Fig. 9(c) depicts the irregular fracture surface caused by fiber microbuckling, delamination, and matrix flaking from the interfacial region which indicates a failure of compression. Fig. 9(d) depicts fibers with shear cusps and cavities, which may have been caused by improper processing and loading resulting in failure of specimen due to fiber impressions, and fibers draw out.

Fig. 10 depicts SEM micrographs of flexurally loaded specimens with various failure modes and ply orientations. Fig. 10(a) demonstrates that

Table 2
Tensile, compressive, flexural and ILSS characteristic of E-glass/epoxy composite laminates.

Fiber orientation	Tensile characteristics					Compressive characteristics			Flexural characteristics			ILSS characteristics				
	UTS (MPa)	±Std. dev	σ_y (MPa)	±Std. dev	E_T (GPa)	±Std. dev	σ_c (MPa)	±Std. dev	E_C (GPa)	±Std. dev	σ_F (MPa)	±Std. dev	E_F (GPa)	±Std. dev	τ_w	τ_s (MPa)	±Std. dev	G_s (GPa)	±Std. dev	γ_{xy} (mm)
0°	684.85	7.85	457.99	2.42	10.21	0.20	18.86	1.57	10.27	0.21	138.43	6.44	9.11	0.15	12.38	15.43	2.02	2.35	0.21	1.99
90°	177.64	3.59	91.90	1.51	5.52	0.67	11.64	1.17	3.87	0.23	12.34	1.08	3.17	0.11	10.75	12.34	0.94	0.37	0.02	3.03
0°/90°	283.82	2.75	183.81	2.72	6.13	0.35	17.42	1.86	9.16	0.05	77.26	5.83	4.73	0.04	11.27	14.26	1.33	1.57	0.03	3.97
±45°	81.84	2.57	33.79	1.01	4.01	0.40	4.60	0.52	6.65	0.23	54.02	4.36	3.02	0.12	9.25	8.02	0.70	0.62	0.05	2.41

the specimen is void-free due to uniform manufacturing pressure. Strong fiber matrix adhesion and low interphase stress concentrations reduce fiber disengagement and fracture. Matrix flaking and interphase delamination are caused by poor interfacial wetting. Fig. 10(b) depicts fibers interphase with openings caused by insufficient interfacial wetting. Due to greater tension in the compressed region, flexural loading causes fiber pullout in the tensile zone [38]. In bi-directional ply-oriented composite specimens, as depicted in Fig. 10(c), inadequate fiber matrix interface interaction causes rapid fiber pullout. Consequently, fiber fracture is prevalent in both tensile and compressive zones, and fiber accumulation results in interphase adhesion. The specimen develops river lines as a result of the curing of the epoxy matrix under a catalyst/accelerator (Fig. 10(c)). Fig. 10(d) demonstrates that fiber/matrix contacts break during shear which draws fibers apart during flexural loading, causing delamination. Delamination is minimal compared to composite specimens with a 90° ply orientation.

The fracture surfaces of the inter-laminar shear strength test specimens were examined using SEM (Fig. 11). This enabled us to determine the strength increase of glass fiber-reinforced epoxy composites at different stacking orders. In Fig. 11(a), there are signs of a thin resin coating covering the smooth and clear fiber surface. This means that the fibers are more strongly bonded to the matrix, and it would take a lot of energy to break the composite. Based on Fig. 11 (b), fibers are dragged out of the epoxy matrix, and fracture bridging results in debonding of the fiber–matrix interface. Some GFs are firmly embedded in the epoxy matrix, while others have a large gap between the matrix and fiber, which means they are debonding at the interface and becoming weaker [33]. When shear happens, constructive cracks form where the fibers meet the matrix. These cracks pull the fibers apart and cause delamination in specimens with 45° fiber orientations, as seen in Fig. 11(d).

3.3. FEA *for composite behaviour prediction*

It is important to predict the mechanical behavior of composite laminates using structural analysis and validate it with experimental data. So, in this study, FEA was carried out to predict the tensile behavior of composites and to ascertain the extent of agreement between prediction and experimental results. The ANSYS commercial software was used to perform the simulation. For isotropic and orthotropic tensile behavior at varied fiber orientations, ASTM D3039-06 [27] was used to develop the E-glass fiber-reinforced epoxy composite specimen model. In Fig. 12 (a), the composite specimen model is 25 mm broad, 250 mm long, 3 mm thick and 150 mm gauge, while Fig. 12 (b) shows the specimen model. The numerical model's Finite Element (FE) mesh was constructed using 54,830 nodes, chexa/cpenta elements with a constant element size of 2 mm, rigid body elements of 6600 in number, and each node carries three degrees of freedom. Based on the model dimension, the domain of the composite was selected in ANSYS by the model dimension. Table 3 shows the FE simulation input material properties.

The boundary conditions were applied to the simulation by anchoring one end of the specimen, which was arrested by translation and rotation about all axes. The specimen's other end was loaded with varying displacements. Fig. 13 illustrates specimen boundary conditions and load. The boundary conditions clamped the tensile specimen in the upper grip in all directions and freed it in the longitudinal direction, where the load is applied. These limitations allowed the tensile test simulation without rotations or bending.

The simulations were performed on the composite specimens at different fiber orientations. Table 4 contrasts the Von Misses stress, strain and displacements of each simulation with the tensile behavior of the specimen. Fig. 14 (a) and (b) depict the displacement and Von Misses stress (principal stress) distribution of the specimen at 90° fiber orientation, as determined by a finite simulation. The FE model for long fiber-reinforced composites with epoxy matrix can approximate the layout distribution of structural units in the direction (z-axis) of loading, as

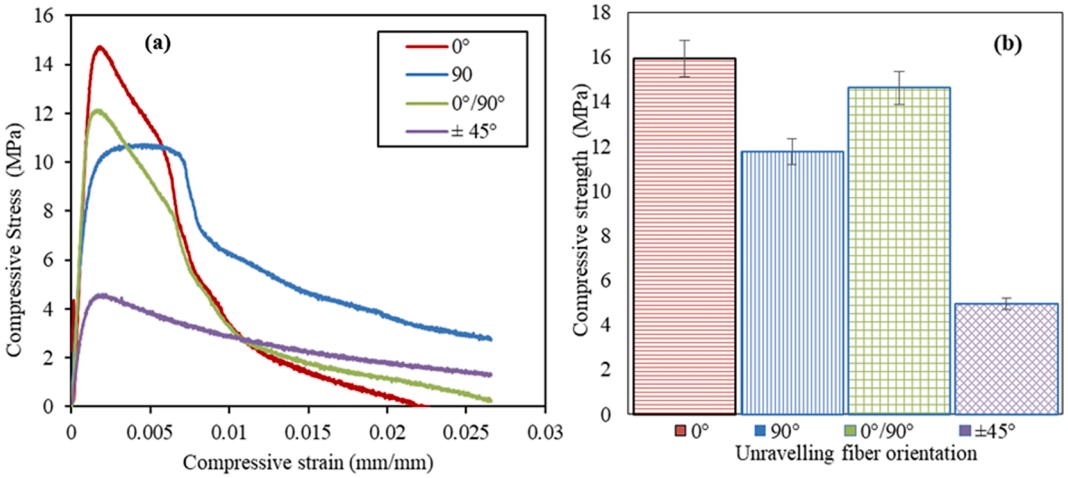

Fig. 5. Characteristic curves of UD-GFRECs (a) Compressive stress–strain, (b) Uncertainty error bar.

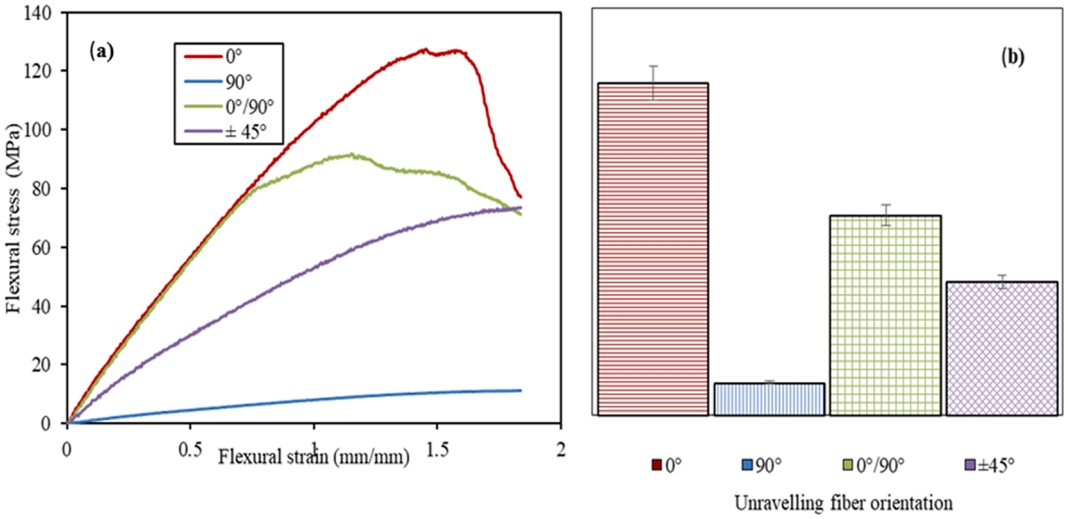

Fig. 6. Characteristic curves of UD-GFRECs (a) Flexural stress–strain, (b) Uncertainty error bar.

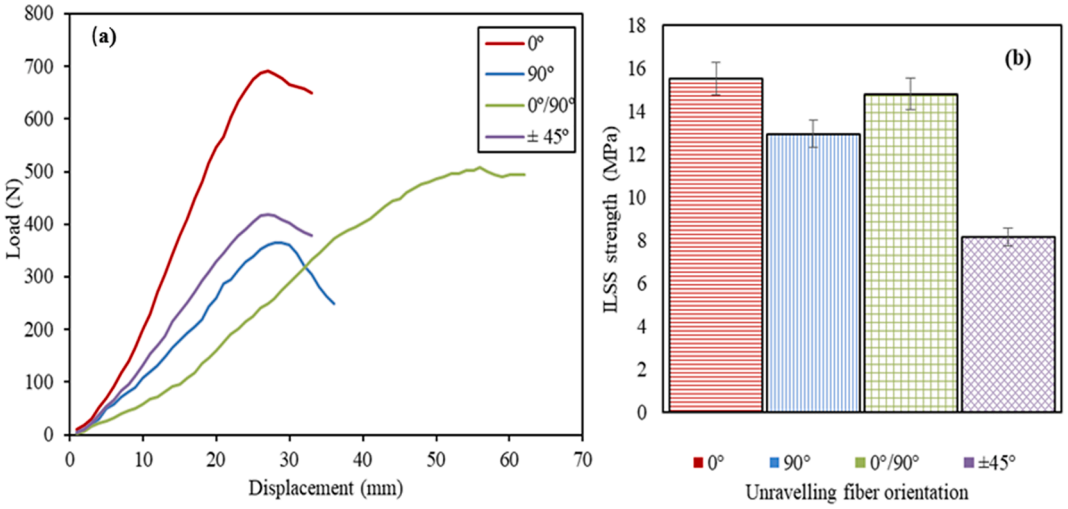

Fig. 7. Characteristic curves of UD-GFRECs (a) Shear load–displacement, (b) Uncertainty bar error.

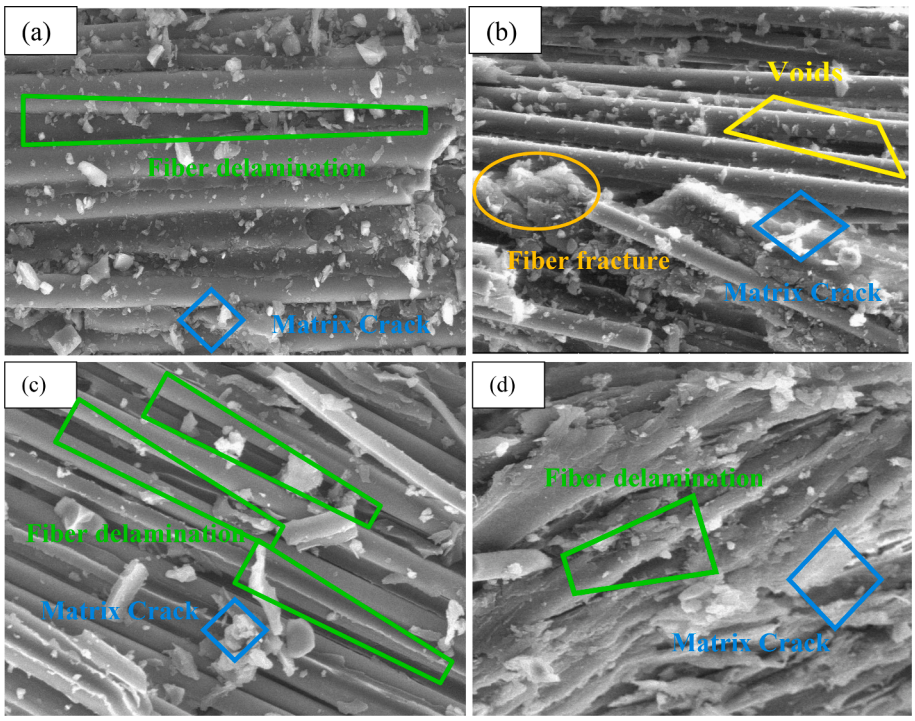

Fig. 8. SEM images showing the fracture pattern of tensile loaded specimens: (a) 0°, (b) 90°, (c) 0°/90°, and (d) ± 45° ply orientations.

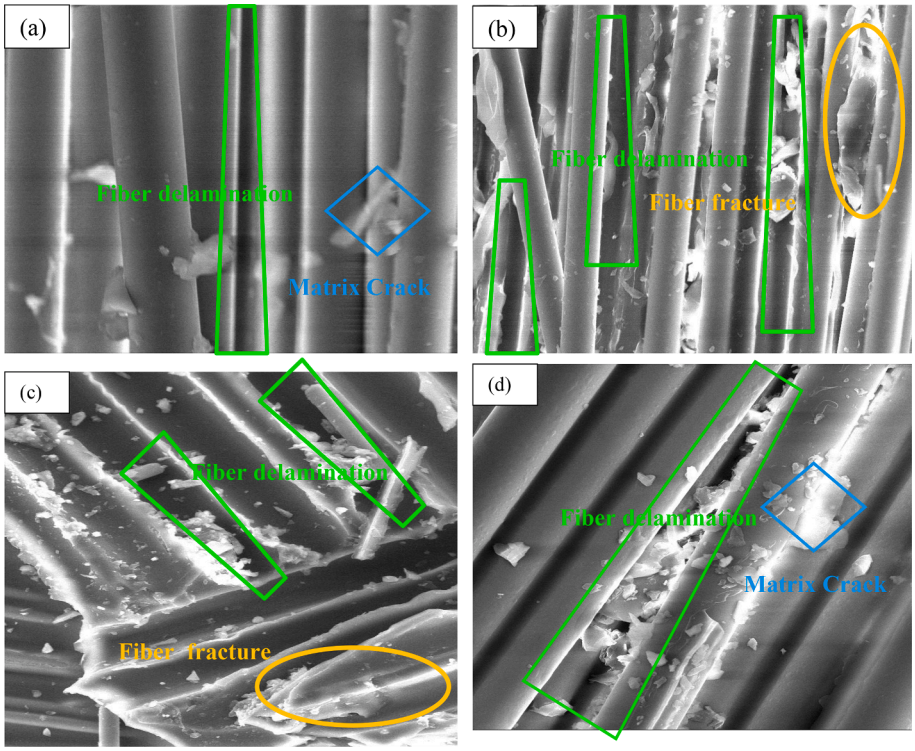

Fig. 9. SEM images of varying fracture pattern of compressively loaded specimens: (a) 0°, (b) 90°, (c) 0°/90°, and (d) ± 45° fiber orientations.

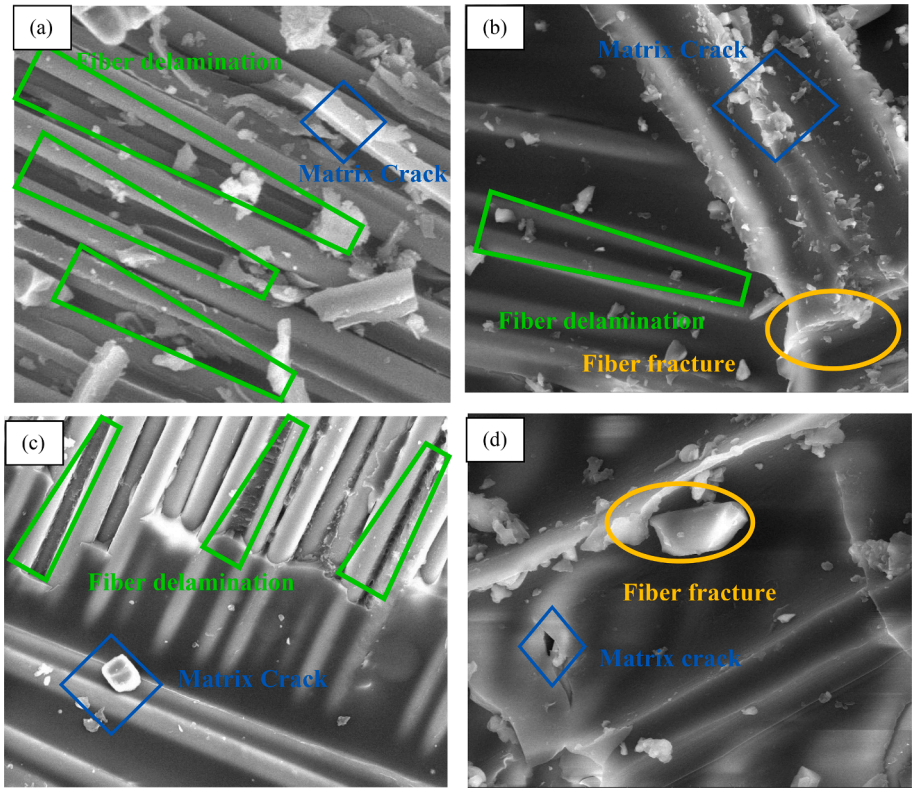

Fig. 10. SEM micrographs of varying failure modes of flexural loaded specimens: (a) 0°, (b) 90°, (c) 0°/90°, and (d) ± 45° ply orientations.

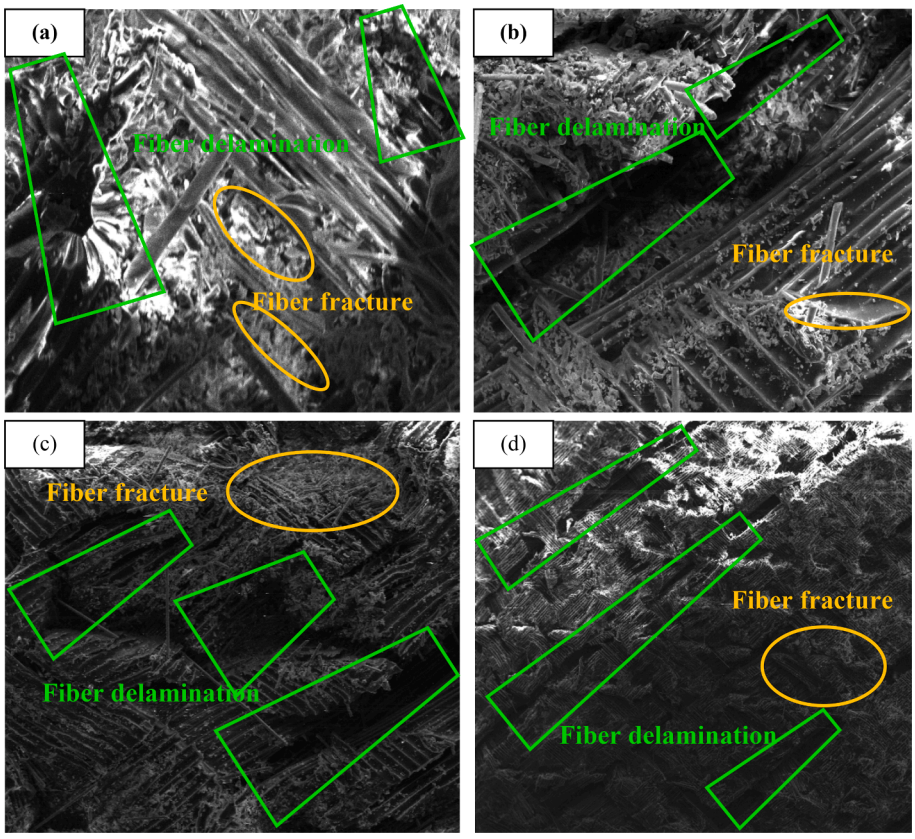

Fig. 11. SEM images of fracture region of short beam shear strength test specimens: (a) 0°, (b) 90°, (c) 0°/90°, and (d) ± 45° fiber orientations.

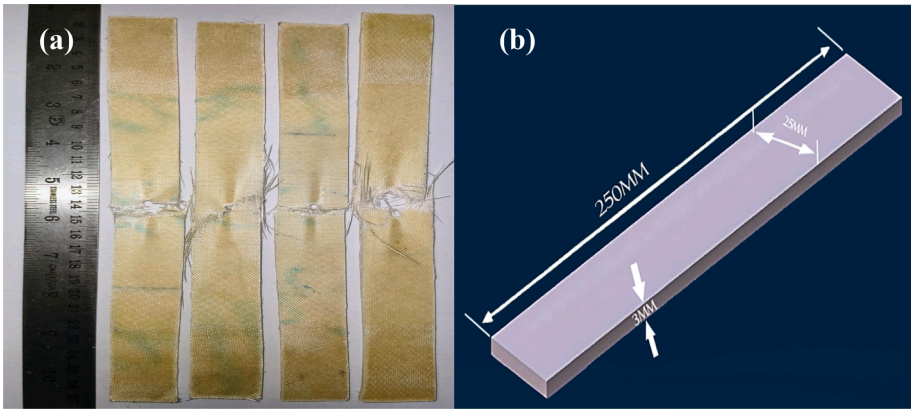

Fig. 12. (a) Fabricated specimens with 0°, 90°, 0°/90°, ±45° fiber orientations, and (b) the specimen model.

Table 3
Material properties for finite element simulation [26].

Material property	UD-GF	Epoxy
E_{11}(MPa)	23,315	37,700
E_{22}(MPa)	6106.23	9130
E_{33}(MPa)	6106.23	9130
G_{12}(MPa)	2166.06	3360
G_{13}(MPa)	2166.06	3360
ν_{12}	0.4271	0.266
ν_{13}	0.4271	0.266
ν_{23}	0.663	0.427
Density (kg/m^3)	2600	1940

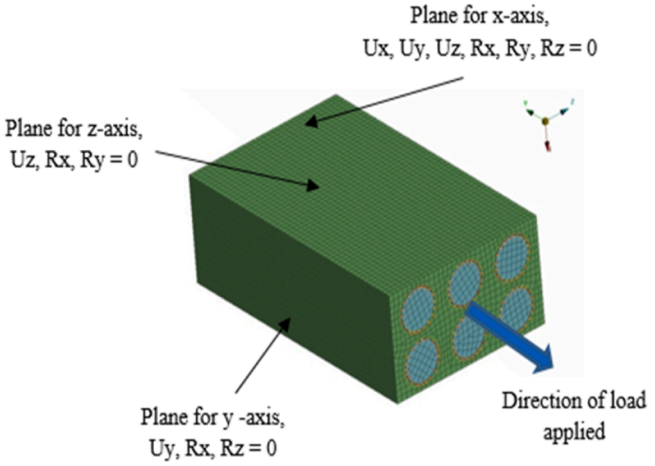

Fig. 13. ANSYS model with boundary conditions and load applied on tensile specimens.

shown in Fig. 14(b) (left), and the Von Misses distribution. Iso-surface sections (Fig. 14 (b) right) determine the primary stress, enabling an analysis of the stress distribution between fibers, matrix, and interphase. At 0.8 % strain and 0.4 V_f the FE model agrees better with the maximal stress values of 177.64 MPa and 190.95 MPa. The distribution of maximal stress between fibers and matrix, which is greatest at the interphase, is depicted in Fig. 14(c). It conforms to the theoretical postulate of fiber–matrix interphase, in which the maximum stress transfers a newly produced component into the interphase, resulting in the synergistic effect of composite structure formation [35]. It also demonstrates that the structural unit's maximum stress is imposed on two instead of six fibers.

The predicted tensile stress–strain behavior of 0°, 90° and 0°/90° fiber-oriented composite laminates is linear elastic up to instantaneous failure without plastic deformation (Fig. 15). The FEA analysis of stress values indicates that the tensile test stress values are greater than the experimental values, as shown in Fig. 15. The maximum stress values obtained experimentally are 747.86 MPa, 187.63 MPa, 283.54 MPa and 81.84 MPa for a strain rate of 0.0025, while the maximum stress values obtained through simulation using ANSYS are 741.64 MPa, 184.08 MPa, 284.54 MPa and 87.22 MPa for a strain rate of 0.0025. Experimental and ANSYS simulation results differ by 0.83 %, 1.89 %, 0.35 % and 6.57 %, respectively, for the considered strain rate. Due to matrix fragmentation, the tensile test specimens begin to yield at 0.25 % strain. In addition, the density of matrix fractures result in a nonlinear response as the load increases [39]. This fracture density reaches saturation at 2.2 % strain, at which point matrix-induced nonlinearity is no longer present. The angles of fiber rotation determine the behaviour of the material, whereas fiber reorientation in the loading direction governs nonlinearity [40]. Experiments reveal that the constant stiffness of a fiber bundle and the derived curves are linear until the applied stress reaches the failure stress, after which there is a sharp decrease in load. The defects in the 90^0 and $\pm 45^0$ fiber orientation samples were both brittle. As seen in Fig. 15, there is not much deviation from experimental and FEA results at 0°, 90°, 0°/90° orientations. At ± 45° orientation, the applied stress induces both tensile and shear stresses in the composite. This leads to complex stress distributions within the material, and accurately modeling these stress states can be challenging. The interaction between different layers in a composite laminate can also affect the mechanical response, especially at off-axis orientations. Delamination can occur at ± 45° orientation, leading to reduced strength and stiffness compared to the theoretical model. And also, at ± 45° orientation, the fibers are

Table 4
Comparison of experimental and FEA results.

Fiber orientation	Displacement (mm)			Strain			Stress (MPa)		
	Exp.	FEA	% error	Exp.	FEA	% error	Exp.	FEA	% error
0^0	11.37	11.37	0.00	0.11074	0.11845	6.96	684.85	714.82	4.38
90^0	1.28	1.279	0.07	0.00804	0.00811	0.87	177.64	190.95	7.49
$0^0/90^0$	6.57	6.568	0.03	0.00703	0.00761	8.25	283.83	284.54	0.25
$\pm 45^0$	1.17	1.168	0.17	0.00802	0.00821	2.36	81.842	76.11	7.00

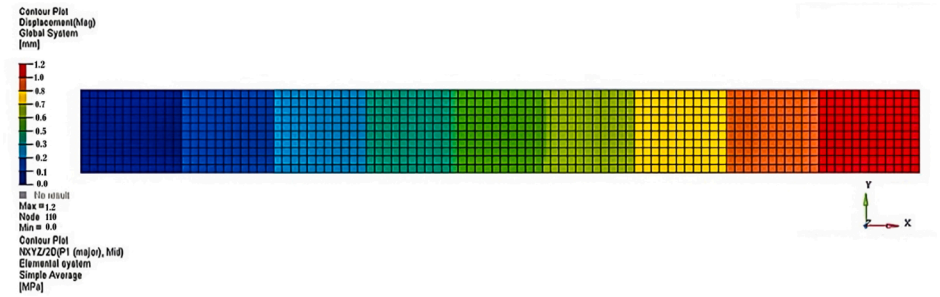

(a)

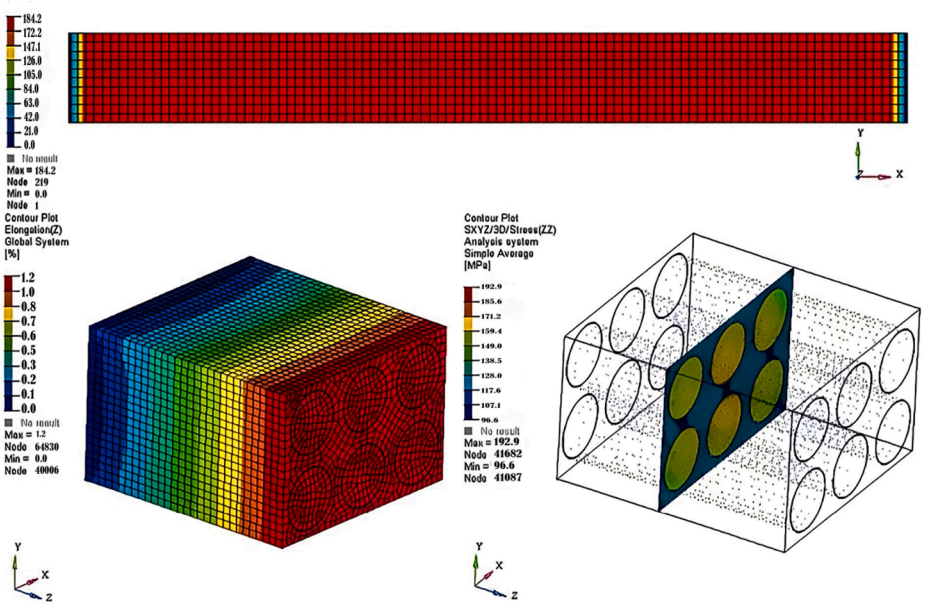

(b)

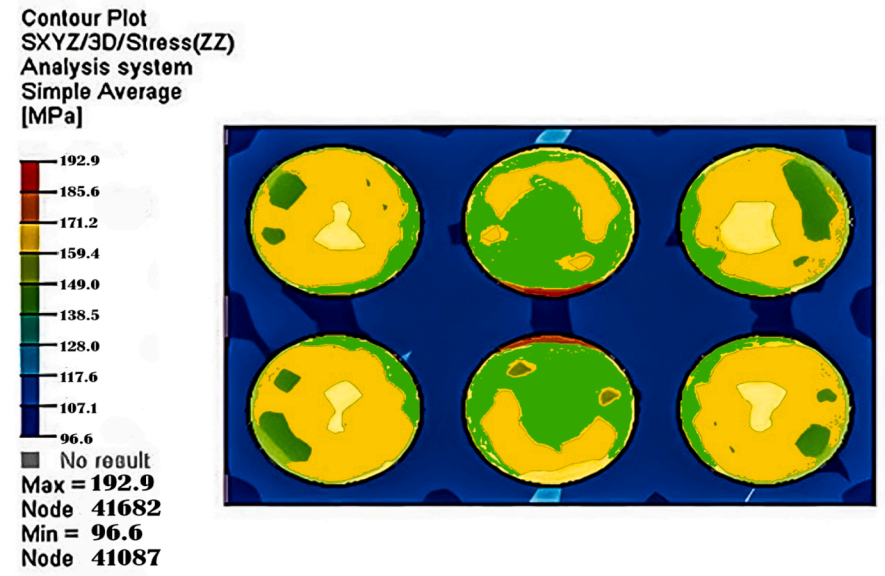

(c)

Fig. 14. (a) Displacement, (b) Von Misses stress of specimen, and (c) Maximum principal stress distribution in the direction of loading (at 90° fiber orientation) obtained through finite simulation.

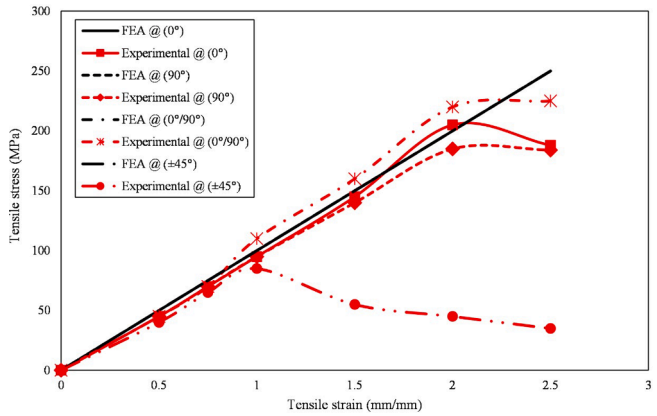

Fig. 15. Comparison of numerical and experimental results of tensile strength behavior of composite laminates at 0°, 90°, 0°/90°, and ± 45° fiber orientation.

oriented diagonally relative to the loading direction. This causes complex interactions between the fibers and the applied stresses, leading to differing mechanical responses.

4. Conclusions

Using the vacuum bagging technique, the present study involved the novel fabrication of laminated composites with an epoxy matrix and glass fibers oriented at 0°, 90°, 0°/90° and ± 45°. The results of the comprehensive investigation from this study make it clear that:

The UTS of composite laminates with different orientations, such as ± 45°, 90° and 0°/90°, was found to be lower than the unidirectional 0° fiber orientation laminate (11.93 %, 25.93 % and 62.14 %, respectively).

The unidirectional 0° fiber-oriented laminate exhibited superior compressive strength, inter-laminar shear strength, and flexural strength, with respective values of 14.846 MPa, 15.62 MPa and 129.62 MPa, when compared to other laminates.

The microstructural analysis has shown that the fracture observed in composite laminates with various ply orientations is due to the debonding of the fiber–matrix interface, fiber pull-out, porosity and river flow lines in the matrix.

The elongation error percentage between the experiment and the simulation was less than 10 %. In addition, it was observed that the results of the FEA are consistent with the empirical findings.

The results of the study indicate that the application of unidirectional glass fiber-reinforced epoxy composites featuring a 0° fiber orientation would be a viable and reliable option for industrial applications. Additional hybrid fiber orientations and optimal design patterns needed for aerospace and structural applications may be investigated further. In addition, the incorporation of nanoparticles in between the orientations of fibers to enhance mechanical properties may also be investigated.

CRediT authorship contribution statement

Seshaiah Turaka: Investigation, Methodology, Validation, Writing – original draft. **Ravikiran Chintalapudi:** Methodology, Resources, Validation. **Narayanan Kannaiyan Geetha:** Conducted the computer simulations. **Bridjesh Pappula:** Methodology, Supervision, Writing – review & editing. **Seshibe Makgato:** Formal analysis, Investigation, Supervision, Writing – review & editing.

Declaration of competing interest

The authors declare that they have no known competing financial interests or personal relationships that could have appeared to influence the work reported in this paper.

Data availability

Data will be made available on request.

References

[1] Desai, Abilash, C. M. Sharanaprabhu, and S. K. Kudari. Experimental investigation on the effects of fiber orientation on translaminar fracture toughness for glass-epoxy composite under mixed Mode I/II load. AIP Conference Proceedings. Vol. 2057. No. 1. AIP Publishing LLC, 2019. https://doi.org/10.1063/1.5085581.

[2] Siddique A, Abid S, Shafiq F, Nawab Y, Wang H, Shi B, et al. Mode I fracture toughness of fiber-reinforced polymer composites: A review. J Ind Text 2021;50(8):1165–92. https://doi.org/10.1177/1528083719858767.

[3] Safi S, Zadhoush A, Ahmadi M, Tehrani SPR. Hybrid silane-treated glass fabric/epoxy composites: tensile properties by micromechanical approach. Iran Polym J 2018;27:1–11. https://doi.org/10.1007/s13726-017-0578-1.

[4] Loganathan TG, Kumar KV, Krishnamurthy R. Assessment of Cyclic Load Induced Energy Dissipation and Damping on GFRP Composite Laminate. Fibers Polym 2020;21:2092–7. https://doi.org/10.1007/s12221-020-9813-z.

[5] Li DS, Dang MG, Jiang L. Experimental investigation on the shear properties and failure mechanism of 3D MWK glass/epoxy composites under compressive loading. Fibers Polym 2020;21:138–47. https://doi.org/10.1007/s12221-020-9312-2.

[6] Dahshan B, El-Habbak AHM, Adly MA, Shazly M. Experimental and numerical study on the tensile, three-point-bending, and interlaminar fracture toughness of GLARE. J Mech Sci Technol 2020;34:3273–81. https://doi.org/10.1007/s12206-020-0719-x.

[7] Taheri-Behrooz F, Shokrieh MM, Sokhanvar H. A new model for the determination of optimum fiber volume fraction under multi-axial loading in polymeric composites. Iran Polym J 2019;28:31–8. https://doi.org/10.1007/s13726-018-0676-8.

[8] Cao D. Enhanced buckling strength of the thin-walled continuous carbon fiber–reinforced thermoplastic composite through dual coaxial nozzles material extrusion process. Int J Adv Manuf Technol 2023;128:1305–15. https://doi.org/10.1007/s00170-023-12014-8.

[9] Cao D, Bouzolin D, Lu H, Griffith DT. Bending and shear improvements in 3D-printed core sandwich composites through modification of resin uptake in the skin/core interphase region. Compos B Eng 2023;264:110912. https://doi.org/10.1016/j.compositesb.2023.110912.

[10] Cao D. Fusion joining of thermoplastic composites with a carbon fabric heating element modified by multiwalled carbon nanotube sheets. Int J Adv Manuf Technol 2023;128:4443–53. https://doi.org/10.1007/s00170-023-12202-6.

[11] Priya IMI, Vinayagam BK. Detection of damages on biaxial GFRP composite material using non-destructive technique. Polym Bull 2021;78(5):2569–603. https://doi.org/10.1007/s00289-020-03228-x.

[12] Sharma P, Mali HS, Dixit A. Mechanical behavior and fracture toughness characterization of high strength fiber reinforced polymer textile composites. Iran Polym J 2021;30(2):193–233. https://doi.org/10.1007/s13726-020-00884-8.

[13] Megahed AAEW, Megahed M. Fabrication and characterization of functionally graded nanoclay/glass fiber/epoxy hybrid nanocomposite laminates. Iran Polym J 2017;26:673–80. https://doi.org/10.1007/s13726-017-0552-y.

[14] Khademi A, Shokrieh MM, Haghighi SE. A novel model to predict the stiffness and strength of unidirectional glass/epoxy composites at different strain rates. J Compos Mater 2020;54(21):2853–71. https://doi.org/10.1177/0021998320903791.

[15] Aghaei M, Shokrieh MM, Mosalmani R. Effect of warp and fill-fiber volume fractions on mechanical properties of glass/epoxy woven fabric composites. J Compos Mater 2020;54(24):3501–13. https://doi.org/10.1177/0021998320914002.

[16] Shanti Kiran Z, Suresh Babu V, Soma Sekhar KVL, Muvvala P, Kameswara Reddy M, Gugulothu S. Tensile and flexural characteristics of an epoxy-glass composite reinforced with Cloisite 15A nanoclay. Iran Polym J 2021;30(8):831–41. https://doi.org/10.1007/s13726-021-00934-9.

[17] Kim CU, Song JI. Effect of hybrid reinforcement on the mechanical properties of vinyl ester green composites. Fibers Polym 2020;21:428–36. https://doi.org/10.1007/s12221-020-9632-2.

[18] Chitturi SK, Shaikh AA. Effect of Stacking Arrangement and Reinforcement Ratio on Impact Behavior of Novel Thermoplastic Embedded Hybrid Composites. Iran J Sci Technol Trans Mech Eng 2021;45:287–97. https://doi.org/10.1007/s40997-020-00384-3.

[19] Wang X, Xie F. Tensile strength and failure behavior of T-stiffened panels with embedded delamination: experimental investigation. Iran Polym J 2021;30(9):897–905. https://doi.org/10.1007/s13726-021-00938-5.

[20] Zhou W, Wei ZY, Wang GF, Han KN, Liu R, Ma LH. Transverse tensile deformation and failure of three-dimensional five-directional braided carbon fiber composites. Fibers Polym 2021;22(4):1099–110. https://doi.org/10.1007/s12221-021-9199-6.

[21] Chen Q, Shou D, Zheng R, Fu B, Fan J, Ma P. Effect of Knitting and Finishing Parameters on the Initial Young's Modulus and Tensile Strength for Polyester Weft Knitted Interlock Fabric. Fibers Polym 2021;22(4):1153–9. https://doi.org/10.1007/s12221-021-9424-3.

[22] Behera A, Dupare P, Thawre MM, Ballal AR. Effect of fatigue loading on stiffness degradation, energy dissipation, and matrix cracking damage of CFRP [±45] 3S composite laminate. Fatigue Fract Eng Mater Struct 2019;42(10):2302–14. https://doi.org/10.1111/ffe.13065.
[23] Mamalis D, Flanagan T, Brádaigh CMÓ. Effect of fibre straightness and sizing in carbon fibre reinforced powder epoxy composites. Compos A Appl Sci Manuf 2018;110:93–105. https://doi.org/10.1016/j.compositesa.2018.04.013.
[24] Mehdikhani M, Gorbatikh L, Verpoest I, Lomov SV. Voids in fiber-reinforced polymer composites: A review on their formation, characteristics, and effects on mechanical performance. J Compos Mater 2019;53(12):1579–669. https://doi.org/10.1177/0021998318772152.
[25] Yang X, Zhan L, Jiang C, Zhao X, Guan C, Chang T. Evaluating random vibration assisted vacuum processing of carbon/epoxy composites in terms of interlaminar shear strength and porosity. J Compos Mater 2019;53(17):2367–76. https://doi.org/10.1177/0021998319829531.
[26] Alam S, Chowdhury MA. Micromechanical analysis of glass fiber reinforced epoxy composites and case study of macro-mechanical observation. Compos Theory Pract 2020;20:23–34.
[27] ASTM D 3039-08 - Standard Test Method for Tensile Properties of Polymer Matrix Composite Materials (2014).
[28] ASTM D3410-21 - Standard Test Method for Compressive Properties of Polymer Matrix Composite Materials with Unsupported Gage Section by Shear Loading (2021).
[29] ASTM D790-17 - Standard Test Methods for Flexural Properties of Unreinforced and Reinforced Plastics and Electrical Insulating Materials (2017).
[30] Li F, Scarpa F, Lan X, Liu L, Liu Y, Leng J. Bending shape recovery of unidirectional carbon fiber reinforced epoxy-based shape memory polymer composites. Compos A Appl Sci Manuf 2019;116:169–79. https://doi.org/10.1016/j.compositesa.2018.10.037.
[31] Pierron F, Vautrin A. The 10 off-axis tensile test: a critical approach. Compos Sci Technol 1996;56(4):483–8.
[32] Van Paepegem W, De Baere I, Degrieck J. Modelling the nonlinear shear stress–strain response of glass fibre-reinforced composites. Part I: Experimental results. Compos Sci Technol 2006;66(10):1455–64. https://doi.org/10.1016/j.compscitech.2005.04.014.
[33] Ng WH, Salvi AG, Waas AM. Characterization of the in-situ non-linear shear response of laminated fiber-reinforced composites. Compos Sci Technol 2010;70(7):1126–34. https://doi.org/10.1016/j.compscitech.2010.02.024.
[34] Agrawal A, Jar PYB. Analysis of specimen thickness effect on interlaminar fracture toughness of fibre composites using finite element models. Compos Sci Technol 2003;63(10):1393–402. https://doi.org/10.1016/S0266-3538(03)00088-5.
[35] Selmy AI, Elsesi AR, Azab NA, Abd El-baky MA. Interlaminar shear behavior of unidirectional glass fiber (U)/random glass fiber (R)/epoxy hybrid and non-hybrid composite laminates. Compos B Eng 2012;43(4):1714–9. https://doi.org/10.1016/j.compositesb.2012.01.031.
[36] Ding S, Zou B, Zhuang Y, Wang X, Li L, Liu J. Hybrid layout and additive manufacturing of continuous carbon/glass fibers reinforced composites, and its effect on mechanical properties. Compos Struct 2023:117133. https://doi.org/10.1016/j.compstruct.2023.117133.
[37] Stephen C, Thekkuden DT, Mourad AHI, Shivamurthy B, Selvam R, Behara SR. Prediction of impact performance of fiber reinforced polymer composites using finite element analysis and artificial neural network. J Braz Soc Mech Sci Eng 2022;44(9):408. https://doi.org/10.1007/s40430-022-03711-8.
[38] Nagoshi T, Harada Y, Nakasumi S, Yamazaki N, Hasegawa K, Takagi K, et al. Inherent cohesive failure of epoxy adhesive in carbon-fiber-reinforced plastic composites revealed by micro-tensile testing and finite element analysis. Compos B Eng 2022;242:110059. https://doi.org/10.1016/j.compositesb.2022.110059.
[39] Dadras H, Barbaz-Isfahani R, Saber-Samandari S, Salehi M. Experimental and multi-scale finite element modeling for evaluating healing efficiency of electro-sprayed microcapsule based glass fiber-reinforced polymer composites. Polym Compos 2022;43(9):5929–45. https://doi.org/10.1002/pc.26850.
[40] Petrů, M., Novák, O, 2018. FEM Analysis of Mechanical and Structural Properties of Long Fiber-Reinforced Composites. Finite Element Method - Simulation, Numerical Analysis and Solution Techniques. InTech. https://doi.org/10.5772/intechopen.71881.